WAVELET DOMAIN ANALYSIS FOR IDENTIFICATION OF VEHICLE AXLES FROM BRIDGE MEASUREMENTS

Pranesh Chatterjee [1], Eugene OBrien [2], Yingyan Li [3], and Arturo González [4]

1. Formerly Post-doctoral Fellow, School of Architecture, Landscape & Civil Engineering, University College Dublin, Ireland.
2. Professor of Civil Engineering, University College Dublin, Ireland.
3. Post-graduate Research Student, School of Architecture, Landscape & Civil Engineering, University College Dublin, Ireland.
4. Lecturer, School of Architecture, Landscape & Civil Engineering, University College Dublin, Ireland.

Abstract

Bridge Weigh-In-Motion (B-WIM) is a process by which the axle and gross vehicle weights of vehicles travelling at highway speeds can be determined from instrumented bridges. The traditional method of attaching strain transducers to the soffit of the bridge and placing axle detectors on the road surface has been replaced here by using additional transducers underneath the bridge for axle detection and Nothing-On-the-Road (NOR). This paper presents a wavelet based analysis of strain signals and shows the efficacy of using wavelets in pattern recognition of these signals. The transformed signals are used to identify axle passage and hence the vehicle velocity and the axle spacing. In addition to numerically generated strains, signals acquired from such a NOR instrumentation of a bridge in Slovenia have been analysed by the method of wavelet transformation to extract axle position information that was not readily detectable using existing methods.

Keywords: bridge, weigh-in-motion, WIM, BWIM, NOR, wavelet, signal processing, axle spacing.

1. Introduction

The main objective of Bridge Weigh-in-Motion (B-WIM) systems is to obtain heavy vehicle weight and classification data using portable technology. This is achieved by first identifying axle passages at two points and hence vehicle velocity and axle spacing. Conventional algorithms can then be used to determine axle and gross vehicle weights. The original algorithm of Moses [1] and variations thereon have been tried and tested in numerous applications [2-5]. In conventional B-WIM systems, two axle detectors on the pavement of each lane of interest provide the times of occurrence of each axle of the vehicle. Pneumatic tubes or tape switches are used for temporary installations but have poor durability and there are safety implications associated with personnel working near traffic. Low grade piezoceramic sensors are much more durable but are expensive and require considerably more installation time which generally requires lane closures.

The concept of a Nothing-On-Road (NOR) B-WIM system, in which only transducers placed beneath the bridge are used to identify axles, is a recent one. A NOR system causes minimal disturbance to normal traffic flow and greatly increases the safety, durability and hence the cost-effectiveness of the installation. However, NOR is only possible if axle locations can be identified in the strain signal, a problem which is the primary focus of this paper.

OBrien & Žnidarič [5] and OBrien et al. [6] demonstrated the effectiveness of NOR B-WIM using orthotropic bridge decks. Orthotropic bridge decks are made from stiffened steel and are generally of low stiffness exhibiting pronounced strain

responses to each axle passage. An optimisation algorithm was developed to identify the axle positions from the slope of the strain response. In field tests, the system demonstrated between Class D+(20) and C(15) accuracy [7,8], depending on the complexity of the algorithm used. These accuracy classes correspond to confidence interval widths of ±20% and ±15% respectively for errors in gross weight. The optimisation algorithm was based on the minimisation of the sum of squares of the differences between the strain responses in two successive spans. This is facilitated by near-identical strain responses in the two spans, which does not apply for two locations in a single span bridge. Further, the strain signature does not show the effect of individual axles as clearly in deeper concrete bridges where there is a greater load dispersion.

In the present study, the strain signals obtained from a numerical model and measurements taken at the Ravbarkomanda bridge in Postojna, Slovenia, are analysed to reveal the latent features of the B-WIM system. The wavelet analytical technique is utilised to extract information from the signals that is often not apparent on visual inspection. The wavelet has emerged as a powerful mathematical tool in the last few decades with applications in different facets of engineering and applied sciences. The unique time-frequency localisation property of the wavelet functions gives it a significant advantage over alternative signal transformations. This paper uses the concept of continuous wavelet transformation to give an accurate identification of the axles of the moving vehicles in the time domain.

2. Wavelet theory

A wavelet-based approach (continuous wavelet transform) is considered in the present study to analyse the NOR strain signals. These strain signals are non-stationary in nature. In the past few decades, wavelet based analysis has proven its efficacy in solving problems which are of a non-stationary random nature. The wavelet transform is probably the most recent solution to overcome the shortcomings of the Fourier transform. The time information is lost in Fourier analysis and the size of the window cannot be changed in a windowed Fourier transform (WFT) or short term Fourier transform (STFT). In a wavelet analysis the use of a fully scalable modulated window solves the signal-cutting problem. There are two types of wavelet transform – continuous wavelet transform (CWT) and discrete wavelet transform (DWT). The window is shifted along the signal and for every position the spectrum is calculated. This process is repeated many times with a slightly shorter or longer window for every new cycle. In the end, the result is a collection of time-frequency representations of the signal or profile, all with different resolutions.

Considerable research has been carried out to develop wavelet functions with specific characteristics to suit different purposes [9-14]. Wavelet analysis can be used to provide an enhanced time-frequency resolution desirable for several applications. It can be effectively used to generate random processes and fields [15,16], simulate earthquake ground motions [17], predict seismic response of storage tanks [18,19], solve partial differential equations [20], and identify damping in multi-degree-of-freedom systems based on time-scale decomposition

[21] and characterise the nonlinear systems [22]. A new representation scheme for random fields based upon the projection onto a biorthogonal wavelet basis was developed [23]. It was shown that biorthogonal processes achieved better decorrelation owing to the fact that fewer filter coefficients were needed to maintain the same support of basis functions when compared to the Daubechies family.

In the present study, CWT has been used for signal processing. The CWT is defined by

$$W_{\psi}x(s,\tau) = \int x(t)\psi_{s,\tau}(t)dt \tag{1}$$

which is a function of two variables, *s* and *τ*. representing the scale and the time factors respectively. These variables *s* and *τ* belong to the set of all integers. The inverse CWT is defined as

$$x(t) = \iint W_{\psi}x(s,\tau)\psi_{s,\tau}(t)d\tau ds \tag{2}$$

where *f(t)* denotes the signal as a function of time, $W_{\psi}x(s,\tau)$ the wavelet coefficients of the signal for a particular scale and time and $\psi_{s,\tau}(t)$ the mother wavelet. The scale factor is the inverse of the frequency. Thus, the wavelets are generated from the single basic wavelet, i.e., mother wavelet, by scaling and translation parameters. The expression for the mother wavelet is given by

$$\psi_{s,\tau}(t) = \frac{1}{\sqrt{|s|}}\psi(\frac{t-\tau}{s}), \tag{3}$$

in which, the term $|s|^{-\frac{1}{2}}$ is used for energy normalisation across different scales. Wavelets are obtained by altering the variables *s* and *τ*. These variables dilate and

translate the mother wavelet to generate various wavelet families. The scale parameter s indicates the width of the wavelet and the translational parameter τ denotes its position in either time or space. The lower is the scale, the more detailed (more localised) is the view. The wavelet moves along the signal with each scale, s and calculates the CWT coefficients at each step, the size of which is determined by the index, τ.

The most important properties are the admissibility and regularity conditions. The admissibility criterion is:

$$\int_{-\infty}^{\infty} \frac{|\hat{\psi}(\omega)|^2}{|\omega|} d\omega < \infty . \tag{4}$$

where $\hat{\psi}_{s,\tau}(\omega)$ is the Fourier transform (FT) of $\psi_{s,\tau}(t)$. The admissibility condition implies that the FT of $\psi(t)$ vanishes at zero frequency, i.e.,

$$|\hat{\psi}(\omega)|^2_{|\omega=0} = 0, \tag{5}$$

which means that wavelets must have a band-pass like spectrum. This is very important to develop an efficient wavelet transform. The regularity conditions imply that the wavelet functions should have some smoothness and concentration in both time and frequency domains.

2.1 Application of wavelets to NOR problems

The CWT cannot be practically computed as it contains an integral (Eq.1) in which the variables are continuous. It is therefore necessary to discretize the transform by sampling the time-frequency plane in such a way that, at lower

frequencies, the sampling rate can be decreased which will save a considerable amount of computation time (this is done by a dyadic sampling grid). A reverse biorthogonal wavelet basis function *rbio2.4* was chosen for the analysis of NOR signals after performing a number of tests with various alternatives. This is a compactly supported biorthogonal spline wavelet for which symmetry and perfect reconstruction are possible. In such a wavelet function, two sets of low pass and high pass filters are used instead of one set as in the case of an orthogonal wavelet. One is used for decomposition or analysis and the other for reconstruction or synthesis; one is the dual of the other. The reconstruction and decomposition wavelet functions *rbio2.4*, with orders 2 and 4 for reconstruction and decomposition, are shown in figures 1(a) and 1(b) respectively. The second value of the two orders, 4 in the case of *rbio2.4*, denotes the number of vanishing moments for the associated wavelet function decomposition.

3. Wavelet analysis of numerically simulated results

A two-dimensional walking beam model has been used to numerically generate strain signals corresponding to a 2-axle tandem travelling at a speed of 75 km/h over a 15 m long simply supported beam – figure 2. This 'vehicle' was chosen because closely spaced axles such as those in tandems and tridems are the most difficult to distinguish from one another in strain signals. The vehicle is assumed to have a total weight of 122 kN with the mass located mid-way between the two axles. It has two degrees of freedom, vertical translation and rotation and the axle spacing is taken to be 1.5 m. Further details are given in Table 1. The second order equation of motion is solved at each time step to find the interaction force between

the axles and the bridge. This is used in the next time step to update the bridge deflection using the Runge-Kutta-Nystrom method [24].

The strains are calculated at points 0.25*L* and 0.75*L*, where *L* is the 15 m length of the beam. Strains, sampled at over 6300 Hz, are shown in figure 3. This example was selected as it has a high amplitude of dynamic vibration which makes is difficult to identify the effect of each axle passing the sensor.

The strain signals at 0.25*L* were analysed using the *rbio2.4* wavelet. Contours of the wavelet coefficients are plotted in figure 4 for a range of scales and times. The axle positions are evident in the figure as two vertical black/grey lines at about 0.18 and 0.25 seconds. While the signals are greater at high scales (30 and more), they are more pronounced at lower scales. A cross-section through figure 4 at a scale of 14 is given in figure 5. The point where each axle passes the sensor can be clearly identified from the two prominent peaks.

The time difference between the arrival of the first axle at 0.25*L* and 0.75*L* was noted from the peaks and the velocity of the vehicle was calculated to be 74.85 km/h, a deviation of 0.2% from the actual value of 75 km/h. From this velocity and the distance between the peaks corresponding to each axle, the axle spacing is calculated to be 1.5012 m, an error of 1.2 mm from the 1.5 m spacing used. The program used for the wavelet analysis of the numerically simulated strain signals was executed in Matlab. With 5000 data points in the time domain, the execution time required was approximately 270 seconds for each signal using a Pentium 4 computer with a 1.4 GHz microprocessor speed and 256 MB RAM.

The wavelet is clearly highly effective at distinguishing the influence of the axle passing the sensor from the effects of vehicle and bridge vibration. However, a numerically generated signal such as this has very "sharp corners" in the static signal superimposed on the vibrational effects. The wavelet is clearly very effective at amplifying such slope discontinuities in the signal. Discontinuities of this type are not present in strains measured in typical concrete bridges due to dispersal of the wheel loads through the depth of the deck.

4. Wavelet analysis of experimental results

Experiments were conducted on the 6 m long Ravbarkomanda box culvert in Postojna, Slovenia in 2004 – see figure 6. The unidirectional traffic was travelling on the culvert in two lanes. The NOR strain signals were measured simultaneously at 16 sensors/channels placed at different points beneath the bridge while traffic flowed at highway speed overhead. Six strains sensors were placed at mid-span to determine axle weights and two, nos. 5 and 12, were placed in the slow lane under the wheel track and off-centre to detect the axles of the moving vehicle. The sampling frequency was 512 Hz. The chief objective of the analysis of these test results is to identify correctly all of the axles on a time scale and hence to determine the vehicle velocity and the axle spacing. To assess the accuracy of the NOR algorithm, trucks from the traffic were stopped and their axle spacings measured using a tape.

For the purpose of the wavelet-based analysis, only the signals recorded at the two off-centre sensors (channels 5 and 12) are considered in this paper. Twenty one vehicle runs are considered, as described in Table 2. The first five are chosen arbitrarily for calibration and the remaining sixteen for testing. Using the measured lengths between axles in the five calibration trucks, the peaks between the transformed signals are used to find the effective length between channels 5 and 12; it is found to be 3.942 m. This is used for the remaining 16 trucks, to convert the time between transformed signal peaks into speeds and axle spacings. The calculated spacings and the differences between these and the manually measured spacings are presented in Table 3. Out of the 47 spacings used for testing, five have errors in calculated position in excess of 0.2 m. Given that tyre contact surface on a road is about 0.3 m, this is considered to be a good result for about 90% of the test vehicles.

Figure 7(a) shows the original signal recorded at channel 5 in response to truck no. 11. Clear peaks are evident for the first four axles but the fifth axle only manifests itself through slight changes in slope in the signal. This signal was transformed using the *rbio2.4* wavelet performing CWT and wavelet coefficients were obtained at different scales. In contrast to the original signal of figure 7(a), there are pronounced peaks for all five axles for the transformed signal of figure 7(b). The wavelet coefficients are illustrated at scale 16. At this frequency, the five axles are the most prominent. It is a key feature of the wavelet approach that the transformation retains the original relationship with time, i.e., the peaks corresponding to the axles occur at the same times in figures 7(a) and (b). The ripples in figure 7(b) only imply that those frequencies also exist in the signal and

they might have occurred due to sudden changes from one frequency component to another. The broad banded peak centered on 1.2 sec in figure 7(b) is probably due to some localized disturbance. However, these ripples or the broad banded peak do not form major spectral components of the signal as it is evident from their low amplitude.

As it has the greatest error in axle spacing, vehicle no. 15 is considered in greater detail. The original and transformed signals at sensor 12 are illustrated in figure 8. The wavelet transformed signal corresponds to the scale 16. While the peak in the original signal corresponding to the fifth axle is indistinct, there are clear peaks for the first four axles. Hence, the axle spacing which gives the greatest error in Table 3 – 2^{nd} to 3^{rd} – can be determined directly from the original signal. It is found that the location of the peaks in this original signal does not differ by more than two scans from those in the transformed signal. Hence, the peak that is the main source of error in axle spacing is present in the original signal. In general for all signals, the peaks in the transformed signal correspond exactly or to within one or two scans of the original signal. Thus, where there are significant inaccuracies in the results, they are not the result of the transformation. Possible explanations for the inaccuracies are measurement errors on site or errors in the original signal. Moreover, the axle locations in the original signal correspond to peaks in the transformed signal quite accurately. However in order to have the same number of peaks in the wavelet transformed signal as the number of axles, the scale has to be chosen properly after a number of trials so that the actual peaks corresponding to the axles become predominant over other small amplitude peaks.

The experimental results have also been analysed using the wavelets belonging to Daubechies (db) family. Figures 9, 10 and 11 show the temporal variation of the wavelet coefficients for scales 6, 16, 24 and 32 using db6, db10 and db20 respectively. These wavelet coefficients have been calculated from the strain signal acquired at sensor 12 during the passage of vehicle 15 (shown in figure 8(a)) over the bridge. Only results of lower values of scales are shown in figures 9-11 because the higher values of scales would dilate the mother wavelet more, resulting in greater incapability in capturing the correct information like the axle detection of the vehicles passing at high speed. It may be observed that too many low amplitude peaks appear at scale 6 in all the figures and these peaks become broader and flatter as scale increases. No prominent peak can be found which may distinctly refer to the obvious presence of the axles and hence detect them. Figure 12 depicts the wavelet coefficients derived from the same signal but using wavelet rbio2.4 for same scales as shown in figures 9-11. On comparing figures 9-12, it may be seen that 5 predominantly distinct peaks appear in figure 12 at scale 16 compared to all other scales. Thus, it is evident that the plot of the wavelet coefficients using rbio2.4 at this scale very closely resembles the original strain signal thereby making the axle detections more reliable both in terms of time and number. The magnified view of the graph at scale 16 of figure 12 is already shown in figure 8(b) and discussed earlier. However, the choice of a particular scale for distinct and proper axle detection may vary and can only be ascertained after a careful investigation of the signal with all probable scales.

5. Conclusions

In this paper, an attempt has been made to analyse strain signals from the soffit of a bridge to detect the passage of vehicle axles overhead. Strain data series generated numerically and collected experimentally are processed using a reverse biorthogonal wavelet, *rbio2.4*. Signals obtained from numerical simulation of a walking beam model are processed using a wavelet based analysis. Even for a difficult signal with a high level of dynamics, there is very close agreement between calculated and assumed vehicle velocities and axle spacings. Experimental data from twenty one trucks with measured axle spacings is also processed. The wavelet approach (using rbio2.4) is highly effective at identifying the presence of an axle and in all cases, it transforms the signal into one in which axles can be clearly identified. Using the first five trucks for calibration, reasonably accurate axle spacings are found for 42 of 47 measurements. Significant errors remain in a few cases. It is reported that, for the latter examples, peaks are present in the wrong locations in the original data and are not a result of the wavelet transformation.

Acknowledgement

The authors gratefully acknowledge the provision of experimental data by the Slovenia National Building and Civil Engineering Institute, ZAG and financial support provided through the Pierse Newman Fellowship.

References

[1] Moses F.. Weigh-in-motion system using Instrumented Bridges. Transportation Engineering Journal, ASCE 1979; 105(3): 233-249.

[2] OBrien, E.J., Žnidarič, A. and Dempsey, A.T., Comparison of Two Independently Developed Bridge Weigh-in-Motion Systems, *Heavy Vehicle Systems*, *Int. J. of Vehicle Design*, 1999, 6(1/4): 147-161.

[3] McNulty, P., and OBrien, E.J., Testing of Bridge Weigh-In-Motion System in Sub-Arctic Climate, *Journal of Testing and Evaluation*, 2003, 31(6): 1-10.

[4] Žnidarič, A., Baumgärtner, W., Bridge Weigh-in-Motion systems – an overview, *Pre-proceedings of the 2nd European Conference on Weigh-in- Motion*, eds. E.J. OBrien & B. Jacob, Lisbon, European Commission, Luxembourg, 1998, 139-151.

[5] OBrien E.J. and Žnidarič A. (Eds.). Weighing-in-Motion of Axles and Vehicles for Europe (WAVE): Report of Work Package 1.2, Bridge WIM Systems. Zavod za gradbenistvo, Slovenia, 2001.

[6] OBrien E.J., Dempsey A.T. and Jacob B.. The Development of a Real Time Orthotropic Bridge Weigh-in-Motion Algorithm. Submitted for publication 2005.

[7] COST 323, European Specification on Weigh-In-Motion of Road Vehicles, EUCO-COST/323/8/99, LCPC, Paris, August, 66 pp, 1999.

[8] Jacob B., OBrien E.J. and Newton W.. Assessment of the Accuracy and Classification of Weigh-in-Motion Systems: Part 2 European Specification. International Journal of Vehicle Design - Heavy Vehicle Systems, 2000; 7(2/3): 153-168.

[9] Stromberg J.O.. A modified Franklin system and higher order spline systems on R^n as unconditional bases for Hardy spaces. In: Bechner W et al., editior. Conf. in honor of A. Zygmund, Wadsworth Math. Series, 1982.

[10] Battle G.. A block spin construction of ondelettes. Part I: Lemarie' functions Comm. Math. Phys. 1987; 110:601-615.

[11] Mallat S.. Multiresolution approximation and wavelets, Trans. Amer. Math. Soc. 1989; 315: 69-88.

[12] Daubechies I.. Ten Lectures on Wavelets, Society for Industrial Applied Mathematics. Philadelphia, Pennsylvania, 1992.

[13] Newland D.E.. An introduction to Random Vibrations, Spectral and Wavelet Analysis. Longman, Harlow, Essex, U.K, 1993.

[14] Basu B.. and Gupta V.K.. Seismic response of SDOF systems by wavelet modeling of nonstationary processes. J. Engrg. Mech. ASCE 1998; 124(10): 1142-1150.

[15] Zeldin B.A. and Spanos P.D.. Wavelet Concepts on Computational Stochastic Mechanics. Journal of Probabilistic Engineering Mechanics 1997; 512: 244-255.

[16] Spanos P.D. and Zeldin B.A.. Monte Carlo treatment of random fields: A broad perspective. Appl. Mech. Rev.1998; 51(3): 219-237.

[17] Iyama J. and Kuwamura H.. Application of wavelets to analysis and simulation of earthquake records. Earthquake Engrg. and Struct. Dynamics 1999; 28: 255-272.

[18] Chatterjee P. and Basu B.. Nonstationary seismic response of tanks with soil interaction by wavelets. Earthquake Engrg. and Struct. Dynamics 2001; 30(10): 1419-1437.

[19] Chatterjee P. and Basu B.. Wavelet-based nonstationary seismic rocking response of flexibly supported tanks. Earthquake Engrg. and Struct. Dynamics 2004; 33(02): 157-181.

[20] Ghanem R. and Romeo F.A.. Wavelet Based Approach for Model and Parameter Identification of Nonlinear Systems. Int. J. of Nonlinear Mechanics 2001; 36(5): 835-859.

[21] Staszewski W.J.. Identification of damping in MDOF systems using time-scale decomposition. J. Sound Vib. 1997; 203(2): 283-305.

[22] Staszewski W.J.. Identification of nonlinear systems using multistage ridges and skeletons of the wavelet transform. J. Sound Vib. 1998; 214(4): 639-658.

[23] Spanos P.D. and Rao V.R.S.. Randon Field Representation in a Biorthogonal Wavelet Basis. J. Engrg. Mech. ASCE 2001; 127(2): 194-205.

[24] Kreyszig E. Advanced Engineering Mathematics. New York: John Wiley & Sons Inc, 1983.

Table 1: Properties of vehicle and bridge models

Vehicle properties			Bridge properties	
Distance between axles	1.5 m		Length of the bridge	15 m
Mass at centre	12 440 kg		Mass per unit length	28 125 kg/m
Moment of inertia	45 000 kg.m^2		2nd moment of area of cross-section	0.527 m^4
Spring stiffnesses (equal)	350 kN/m		Modulus of elasticity	35×10^9 N/m^2
Damping coefficients (equal)	7 kNs/m			

Table 2: Physical characteristics of the trucks on Ravbarkomanda bridge as measured by tape and static scales (vehicles shown shaded used for calibration)

Vehicle No.	GVW (kN)	No. of axles	Measured axle spacing (m)			
			1^{st} to 2^{nd}	2^{nd} to 3^{rd}	3^{rd} to 4^{th}	4^{th} to 5^{th}
1	331	4	1.80	1.94	1.40	
2	153	5	3.60	5.90	1.33	1.33
3	343	5	3.49	5.50	1.18	1.18
4	366	5	3.71	5.87	1.32	1.32
5	122	2	4.45			
6	312	5	3.81	5.50	1.32	1.31
7	380	5	3.30	1.36	4.71	1.32
8	316	5	3.72	5.81	1.31	1.31
9	272	5	3.90	5.84	1.31	1.31
10	114	2	4.60			
11	377	5	3.81	5.85	1.31	1.31
12	95	3	5.08	7.51		
13	262	5	3.59	5.72	1.33	1.31
14	377	5	3.52	5.79	1.31	1.31
15	179	5	3.19	6.06	1.32	1.31
16	163	2	4.31			
17	73	2	4.21			
18	391	5	3.70	5.64	1.31	1.31
19	371	5	3.52	5.69	1.32	1.31
20	120	2	4.16			
21	55	2	4.18			

Table 3: Calculated axle spacings from wavelet analysis and errors (m)

No.	Calculated axle spacing (m)				Error in calculated axle spacing (m)			
	1st to 2nd	2nd to 3rd	3rd to 4th	4th to 5th	1st to 2nd	2nd to 3rd	3rd to 4th	4th to 5th
1	1.81	2.24	1.36		-0.01	-0.30	0.04	
2	3.52	5.86	1.32	1.36	0.08	0.04	0.01	-0.03
3	3.54	5.45	1.21	1.19	-0.05	0.05	-0.03	-0.01
4	3.69	5.82	1.38	1.38	0.02	0.05	-0.06	-0.06
5	4.47				-0.02			
6	3.94	5.35	1.38	1.38	-0.13	0.15	-0.06	-0.07
7	3.24	1.41	4.73	1.36	0.06	-0.05	-0.02	-0.04
8	3.75	5.71	1.35	1.35	-0.03	0.10	-0.04	-0.04
9	3.96	6.08	1.37	1.36	-0.06	-0.24	-0.06	-0.05
10	4.73				-0.13			
11	3.96	5.77	1.48	1.40	-0.15	0.08	-0.17	-0.09
12	4.99	7.43			0.09	0.08		
13	3.47	5.45	1.16	1.40	0.12	**0.27**	0.17	-0.09
14	3.36	5.40	1.17	1.17	0.16	**0.39**	0.14	0.14
15	3.12	5.43	1.49	1.09	0.07	**0.63**	-0.17	**0.22**
16	3.79				**0.52**			
17	4.22				-0.01			
18	3.66	5.64	1.41	1.41	0.04	0.00	-0.10	-0.10
19	3.58	5.55	1.26	1.26	-0.06	0.14	0.06	0.05
20	4.07				0.09			
21	4.12				0.06			

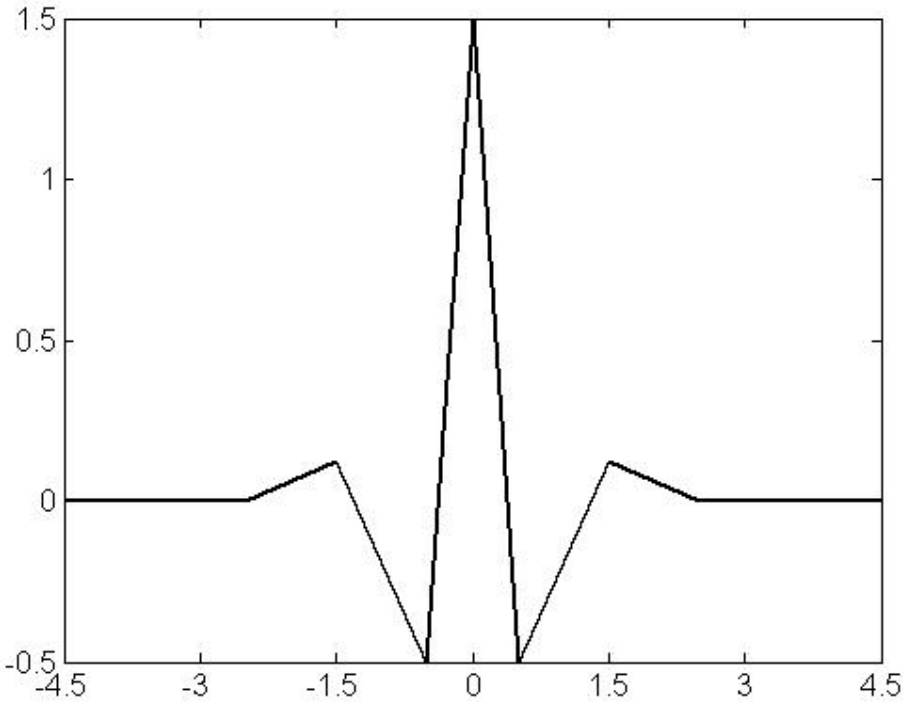

Figure 1a: Decomposition wavelet function, $\psi(t)$ for mother wavelet *rbio2.4*

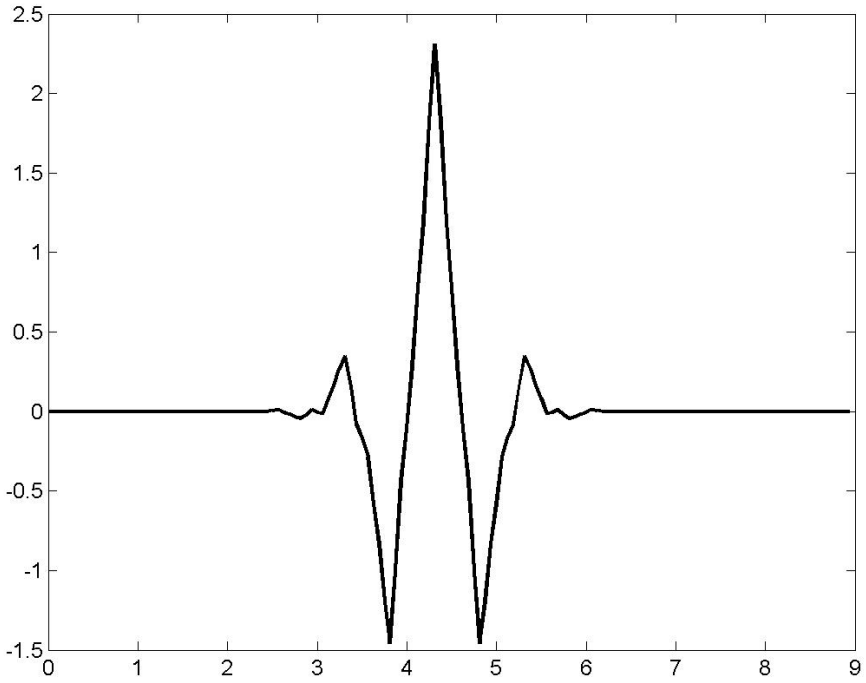

Figure 1b: Reconstruction wavelet function, $\psi(t)$ for mother wavelet *rbio2.4*

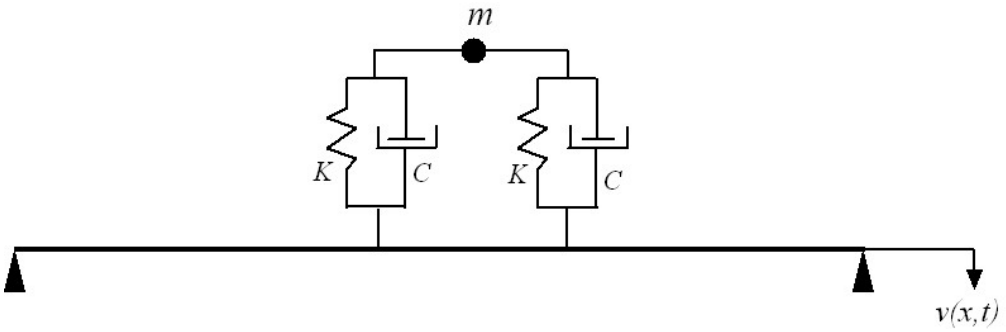

Figure 2: Vehicle model

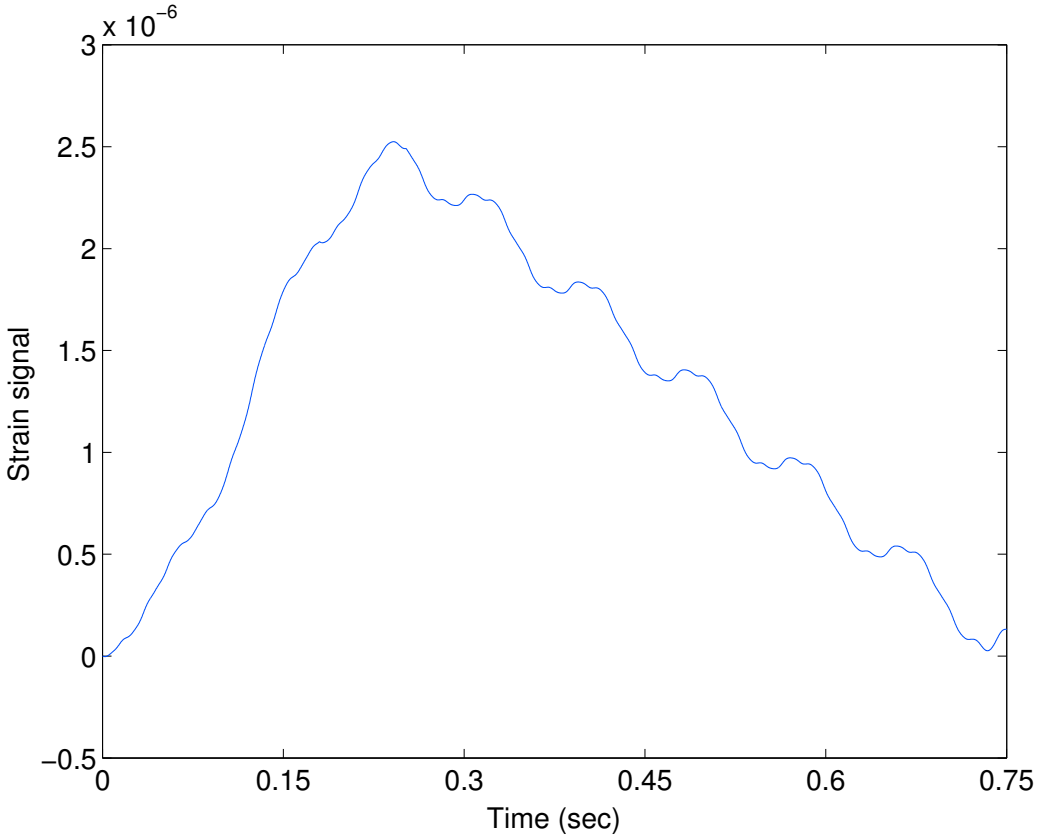

(a) Original strain signal, at $0.25L$

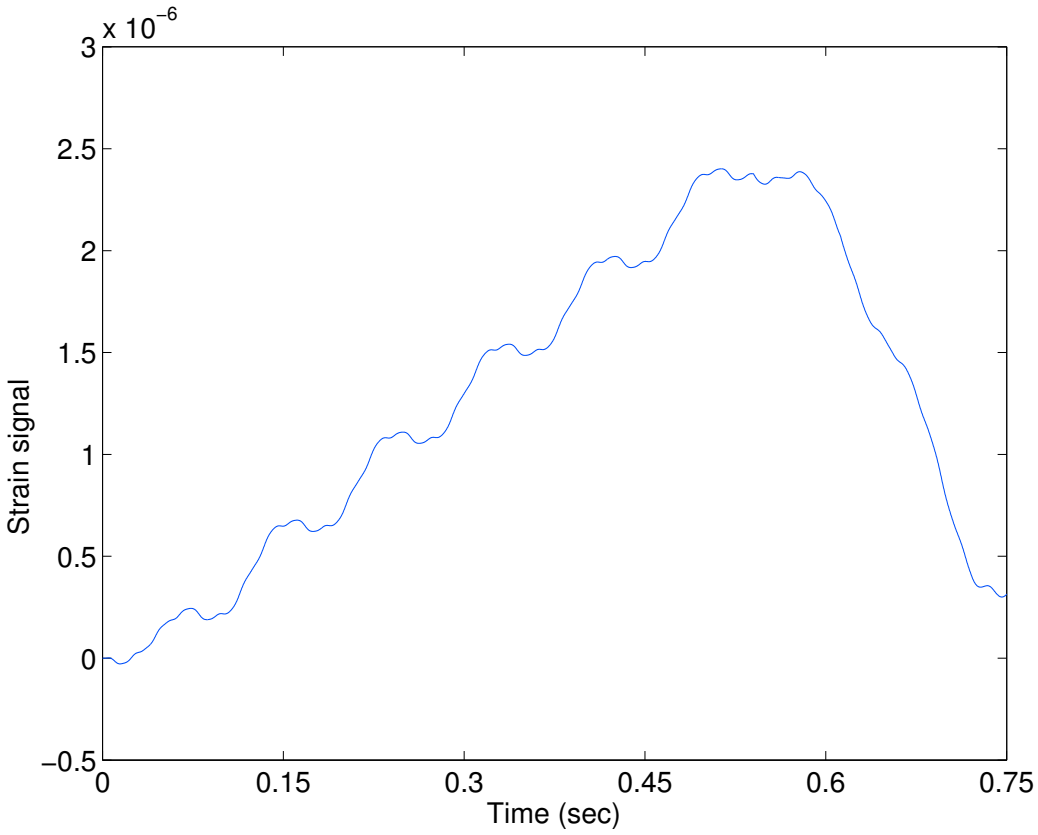

(b) Original strain signal, at $0.75L$

Figure 3: Strain signals obtained from numerical model of beam (L = span = 15 m)

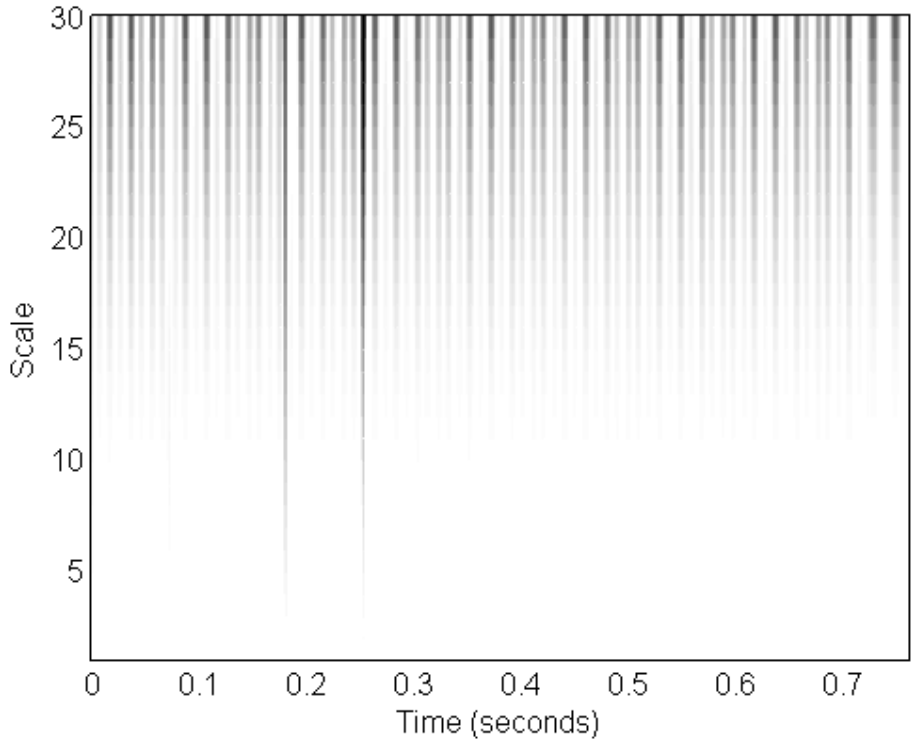

Figure 4: Contours of wavelet coefficients for range of scales (vertical axis) and times (horizontal axis)

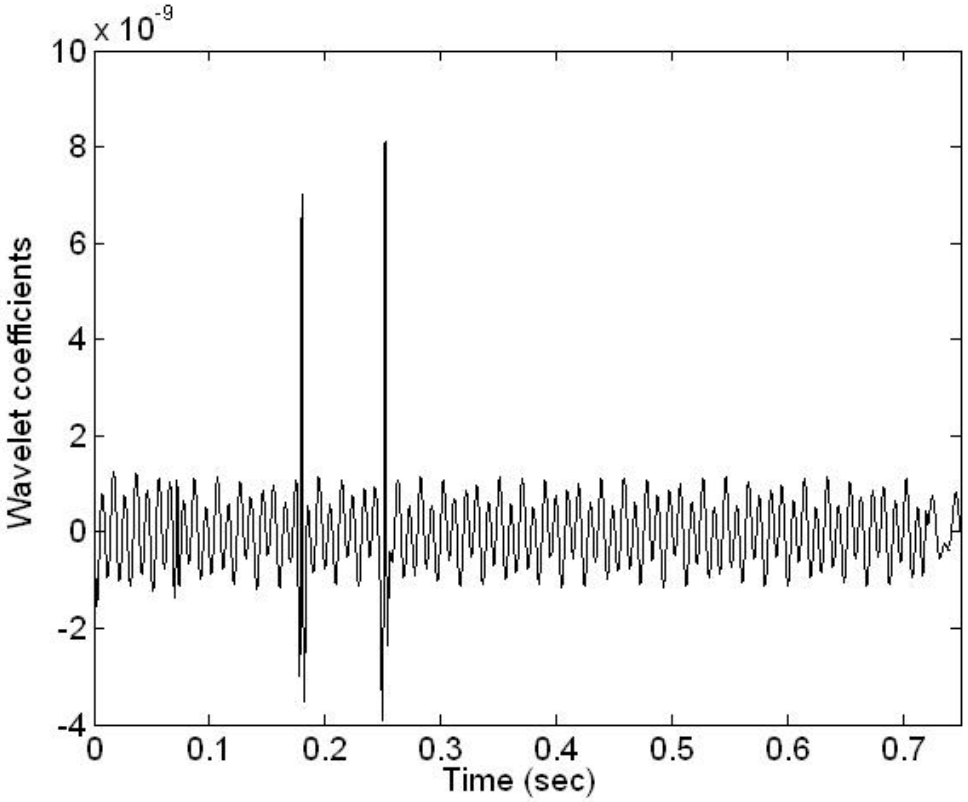

Figure 5: Wavelet coefficients at 0.25*L* for scale of 14

Figure 6: Ravbarkomanda bridge (photograph courtesy of ZAG Slovenia)

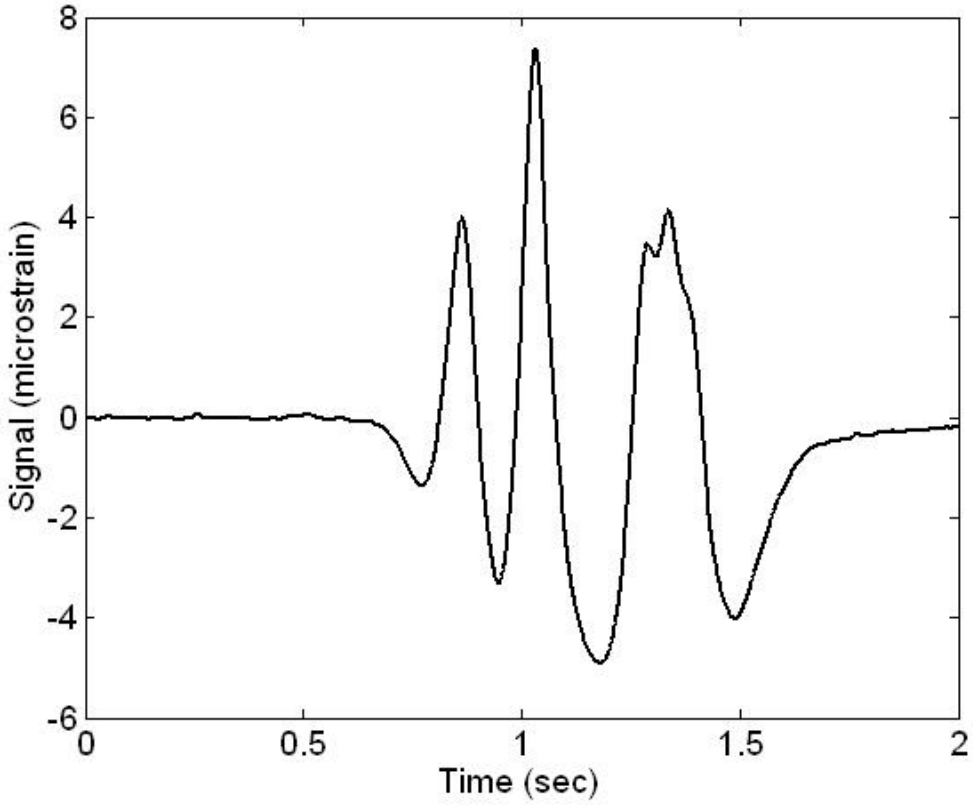

(a) Original strain signal

Figure 7

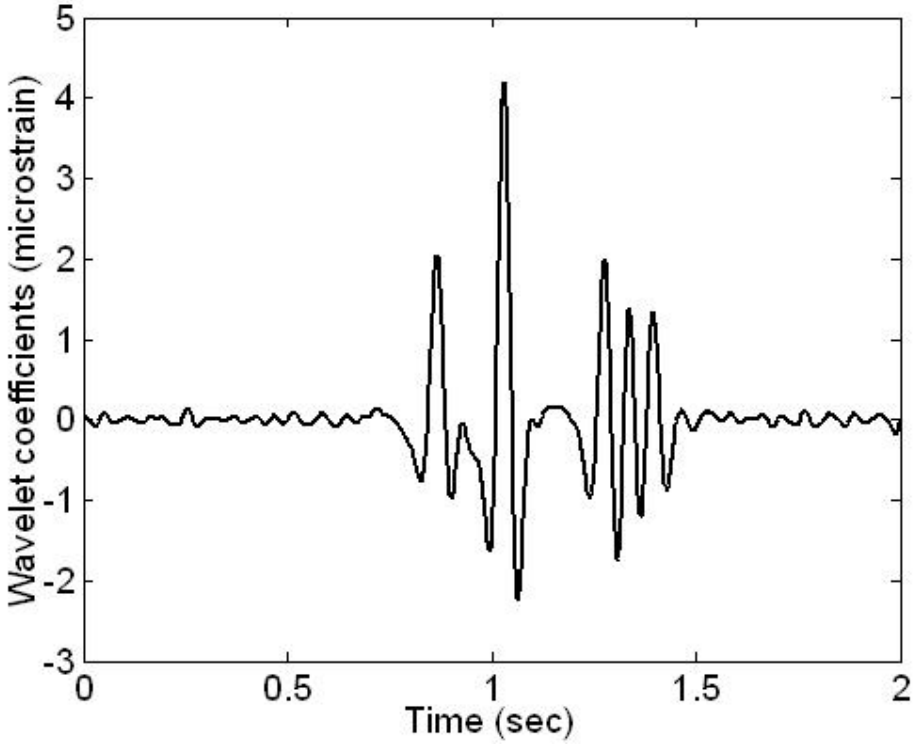

(b) Strain signal after wavelet transformation

Figure 7: Strain signal and wavelet transform, vehicle no. 11

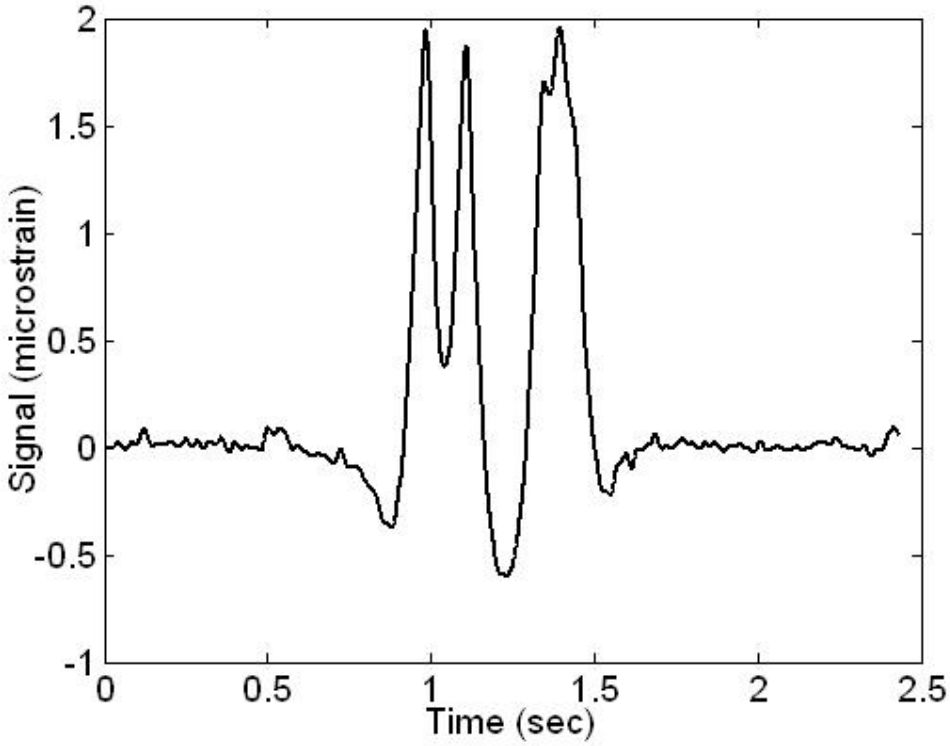

(a) Original strain signal

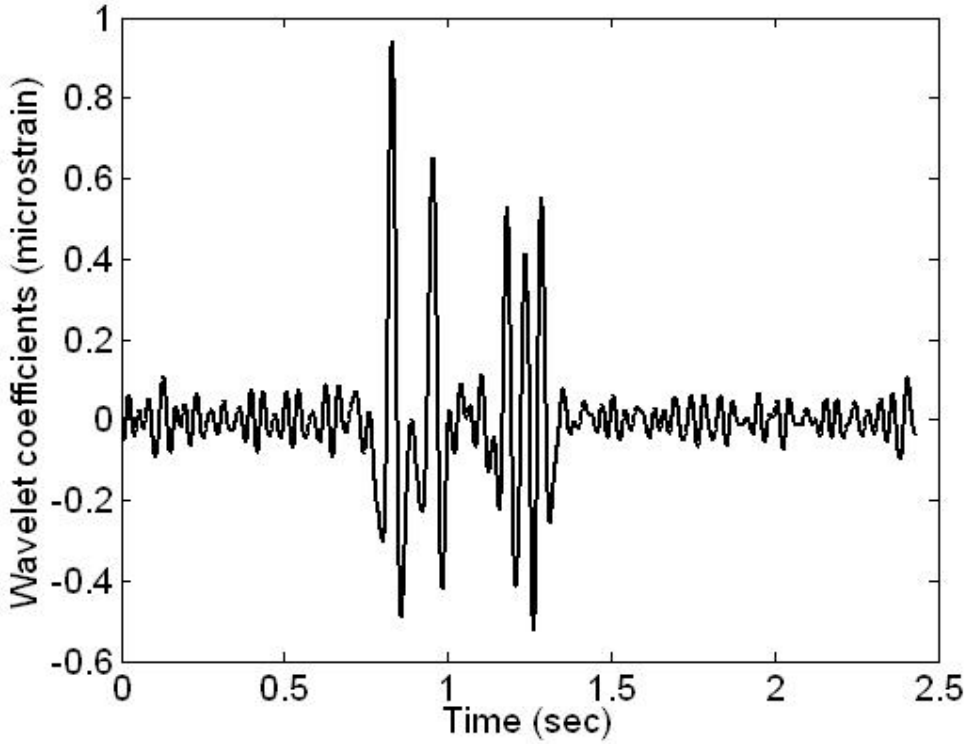

(b) Strain signal after wavelet transformation

Figure 8: Strain signal and wavelet transform, vehicle no. 15

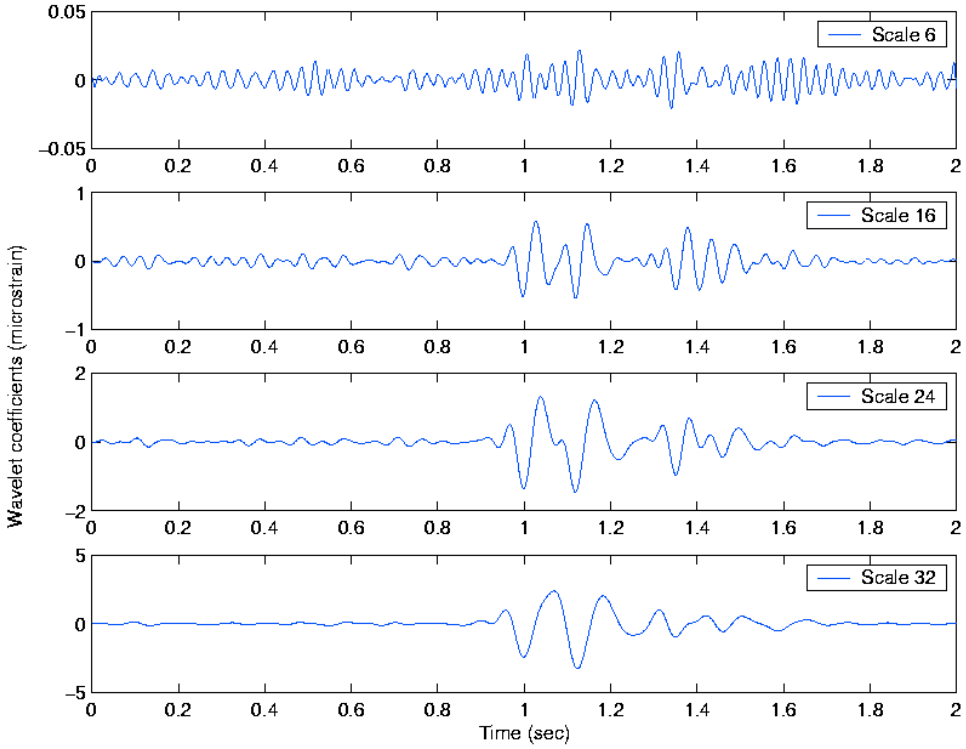

Figure 9: Wavelet coefficients of signal shown in figure 8(a) using db6

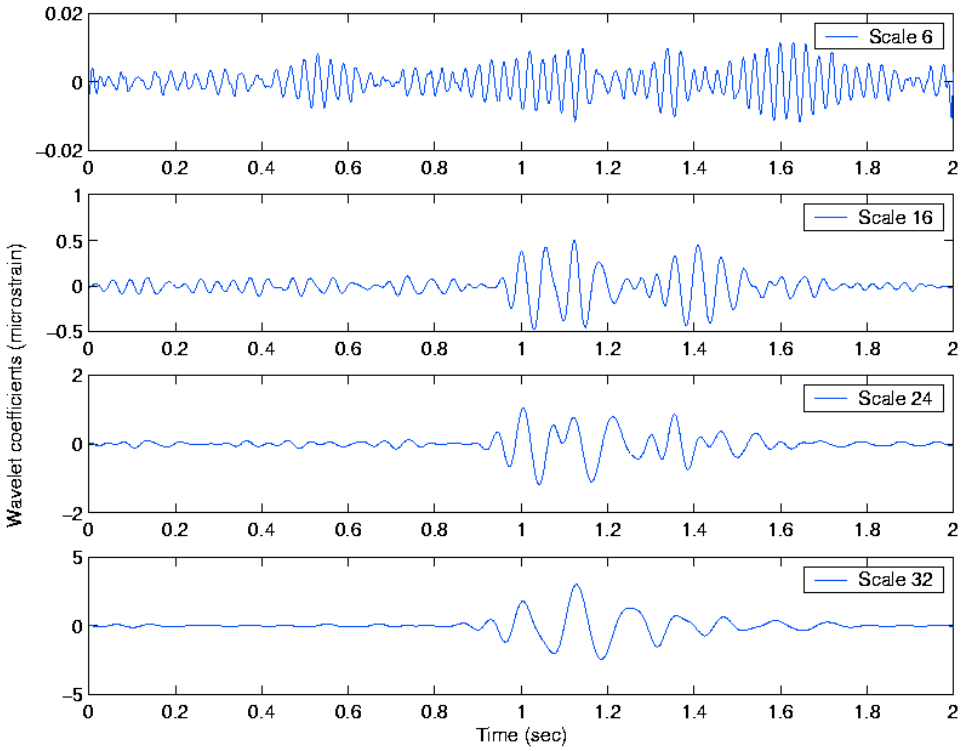

Figure 10: Wavelet coefficients of signal shown in figure 8(a) using db10

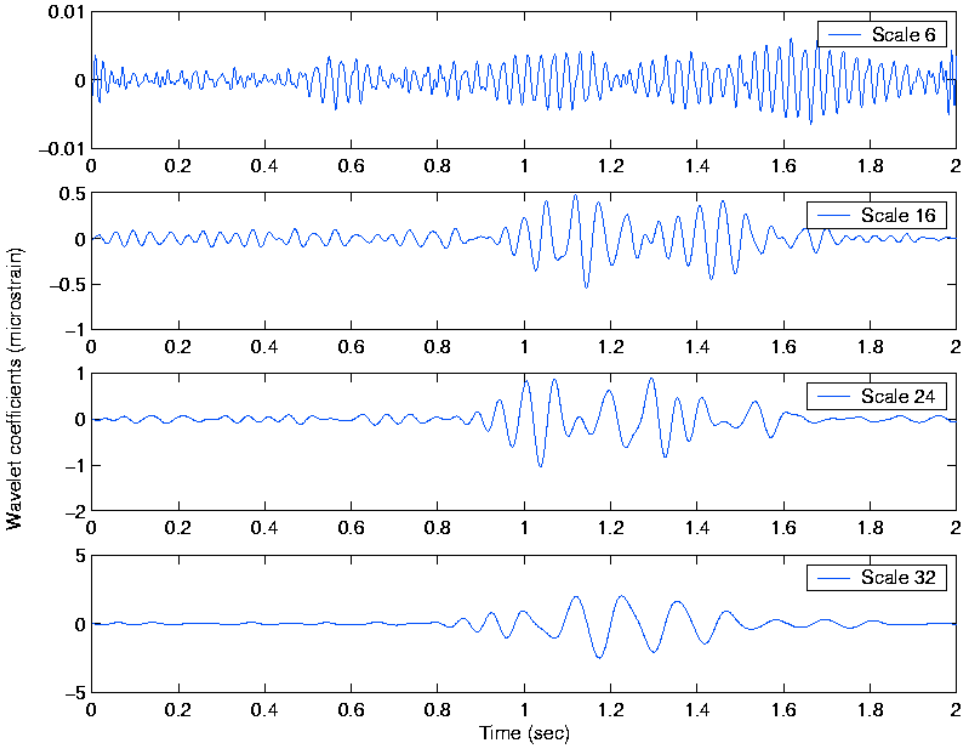

Figure 11: Wavelet coefficients of signal shown in figure 8(a) using db20

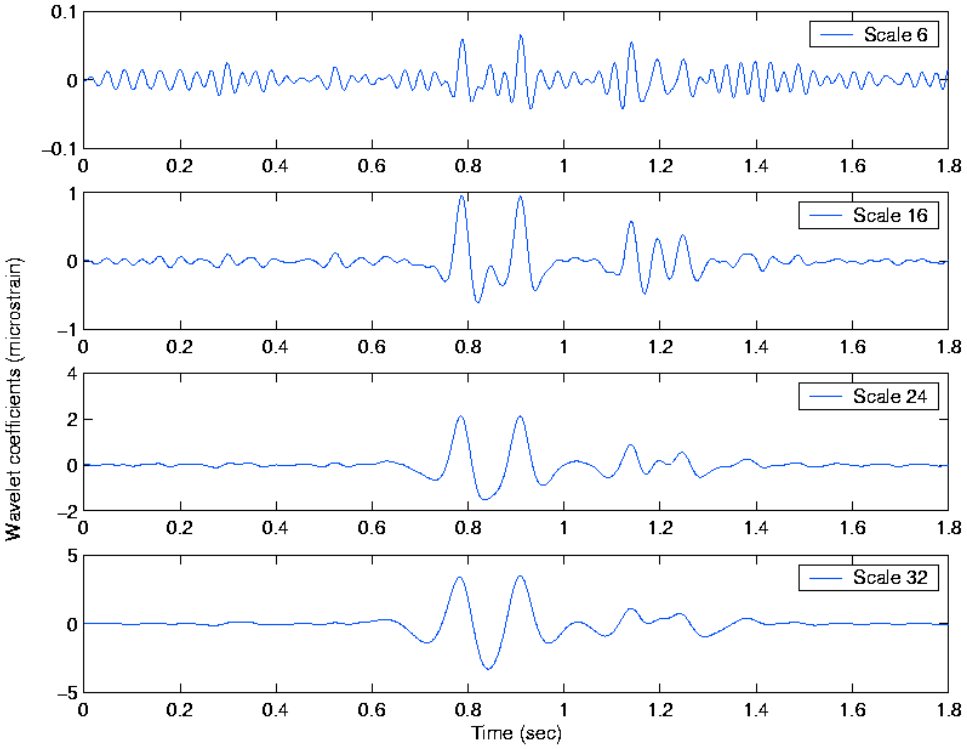

Figure 12: Wavelet coefficients of signal shown in figure 8(a) using rbio2.4